

Developing Neocortex Organization and Connectivity in Cats Revealed by Direct Correlation of Diffusion Tractography and Histology

Emi Takahashi¹⁻³, Guangping Dai³, Glenn D. Rosen⁴, Ruopeng Wang³, Kenichi Ohki^{5,6}, Rebecca D. Folkerth⁷, Albert M. Galaburda⁴, Van J. Wedeen³ and P. Ellen Grant^{1-3,8}

¹Division of Newborn Medicine, Department of Medicine, Children's Hospital Boston, Harvard Medical School, Boston, MA 02115, USA, ²Fetal-Neonatal Imaging and Developmental Science Center, Boston, MA 02115, USA, ³Department of Radiology, Massachusetts General Hospital, Athinoula A. Martinos Center for Biomedical Imaging, Charlestown, MA 02119, USA, ⁴Department of Neurology, Beth Israel Deaconess Medical Center, ⁵Department of Neurobiology, Harvard Medical School, Boston, MA 02115, USA, ⁶Department of Molecular Physiology, Kyushu University Graduate School of Medical Sciences, Higashi-ku, Fukuoka, Japan 812-8582, ⁷Department of Pathology and ⁸Department of Radiology, Children's Hospital Boston, Harvard Medical School, Boston, MA 02115, USA

Van J. Wedeen and P. Ellen Grant equally contributed as senior authors.

Address correspondence to Emi Takahashi, PhD, Division of Newborn Medicine, Department of Medicine, Children's Hospital Boston, Harvard Medical School, Boston, MA 02115, USA. Email: emi@nmr.mgh.harvard.edu.

The immature cortex (cortical plate [CP]) and underlying subplate (SP), a transient cell layer just below the CP, play critical roles in the formation of intracerebral connections. The purpose of this study was to examine the diffusion characteristics of the developing cortex and subcortical structures and compare to histology. We obtained high-resolution diffusion spectrum images of postnatal day (P) 0 (newborn), P35 (pediatric), and P100 (adult) cat brains, performed tractography analysis, and correlated with histological findings. Tractography revealed radial organization and radial afferent/efferent tracts not only in the CP but also in external SP at P0. Radial organization persisted only in the cortex but decreased at P35 and P100. Radial organization correlated with radial cellular organization, with highest cellular density at P0 (Cresyl Violet staining). At P0, the internal SP contained abundant corticocortical and projection tractography pathways, crossing at wide angles in areas with no myelination by Luxol Fast Blue staining. At P35 and P100, increased directional coherence of white matter was observed, with fewer local tracts, but more long association pathways. These results suggest that diffusion tractography can differentially characterize internal and external SP zones and their transition into mature cortical pathways.

Keywords: cat, cortical plate, development, diffusion spectrum imaging, upplate, tractography

Introduction

During the late fetal period and early preterm period, the most prominent transient layer is the subplate (SP) zone, located between the immature cortex (cortical plate [CP]) and the immature white matter (intermediate zone [IZ]), which contains awaiting thalamocortical afferent fibers that cross one another (Kostovic and Rakic 1990; Allendoerfer and Shatz 1994; O'Leary et al. 1994; Ulfing et al. 2000). The SP develops around prenatal week (W) 13 in humans and gradually disappears after W32–34 (Kostovic and Rakic 1990; Ulfing et al. 2000). In the cat, the SP develops around embryonic day (E) 25 and begins to disappear around postnatal day (P) 60, with 90% of SP neurons gone by P120 (Allendoerfer and Shatz 1994; O'Leary et al. 1994; Issa et al. 1999). When fully present, the SP in the cat is reported to be equal to the CP in thickness (Allendoerfer and Shatz 1994). Although there is still debate about the exact boundaries of the SP during development in the cat, in this study, we use the term SP for the region

immediately below the CP at P0, as defined histologically (Allendoerfer and Shatz 1994).

The SP plays a crucial role in helping immature thalamocortical axons find their destinations and form appropriate synaptic connections in the CP. The SP initiates the permanent, sensory-driven circuitry established around prenatal W24 in humans (Kostovic and Jovanov-Milosevic 2006) and around E50 in the cat (Johnson and Casagrande 1993; Hermann et al. 1994). The SP is therefore an area that cannot be overlooked if one is to understand the development of cortical connectivity.

By virtue of the recent technical advances in diffusion tensor magnetic resonance imaging (DTI), we can now study global fiber pathways in the brain (Basser et al. 1994, 2000; Pierpaoli et al. 1996; Cellerini et al. 1997; Makris et al. 1997; Conturo et al. 1999; Jones et al. 1999; Mori et al. 1999). DTI is based on measurements of the apparent diffusion of water molecules in brain tissue and assumes that water diffusivity is represented by an ellipsoid tensor in each voxel. Thus, for each voxel, typically 8 mm³, it is assumed that there is only one major direction of water diffusivity. Diffusion fractional anisotropy (FA) is one of the indices derived from DTI that represents the magnitude of this directional bias, with a value of 1 representing the theoretical limit of all diffusion in only one direction and 0 representing no directional diffusion bias. This preferred directionality of diffusion may be dictated by a structural bias, such as the direction taken by a bundle of axons. In this context, low FA corresponds to a low underlying preferential orientation of fibers or a mix of fibers traveling in several directions (such as crossing fibers). In addition, although conventional magnetic resonance imaging (MRI) techniques have demonstrated signal changes that occur with myelination (Barkovich et al. 1988; Van der Knaap and Valk 1990; for review Paus et al. 2001), DTI measures such as FA provide a complimentary method for quantifying the myelination of white matter (Rutherford et al. 1991; Sakuma et al. 1991; Huppi et al. 1998; Neil et al. 1998; Baratti et al. 1999; for review Neil et al. 2002).

The use of algorithms to reconstruct 3D white matter trajectories from DTI data (Basser et al. 1994; Conturo et al. 1999; Jones et al. 1999; Mori et al. 1999) is often referred to as diffusion tractography. There are many tractography algorithms, but the most commonly used streamline algorithm creates "tracts" by connecting adjacent voxels if their directional bias (FA) is above a threshold level, and if the primary

direction of their diffusion bias differs by less than a threshold angle, typically between 35° and 60°. Thus, diffusion tractography permits examination 1) of major white matter axonal pathways (association, interhemispheric, and projection), 2) throughout the entire brain, and 3) in vivo; such examination is not achieved using conventional MRI techniques.

Many ex vivo diffusion studies of developing animal (Zhang et al. 2003, 2005; Huang et al. 2006, 2008; Kroenke et al. 2007; D'Arceuil et al. 2008; Kuo et al. 2008; Takahashi et al. 2010) and fetal human brains (Huang et al. 2009) have been published. These studies reported that FA values increase in the white matter with age. Some investigators have also performed diffusion tractography (Zhang et al. 2003; Huang et al. 2006, 2009; D'Arceuil et al. 2008) showing the development of major white matter pathways. However, these studies did not illustrate the detailed cortical fiber pathways in relation to the transient layer structures, probably because of the existence of low FA areas, crossing fibers, and regions where fibers take sharp turns (almost 90°) as they enter the cortex. All these factors can result in inappropriate termination of fiber tracking.

In our previous study (Takahashi et al. 2010), we showed development of major fiber bundles (thalamocortical, cingulum, and some corticocortical pathways). Here we focus on the CP and underlying SP. In the CP, we show decreasing radial organization with decreasing neuronal density on Cresyl Violet staining. In this article, we also show that the SP consists of an outer radially organized region and an inner region containing crossing tracts. We are able to detect this structure in the SP even when myelin was not detected on Luxol Fast Blue. Therefore, our current article builds on our prior study providing additional original information critical to understanding the evolution of the CP and SP into the mature cortex and subcortical white matter.

To study the evolution of the CP and SP into the mature cortical and immediately subcortical structure, we compared diffusion spectrum imaging (DSI) tractography, several diffusion measures including FA and apparent diffusion coefficients (ADC), and histological measures in postmortem cat brains aged from newborn to adult. There were 3 reasons behind our choice of the cat brain for these investigations: 1) ex vivo human fetal brains are not easily obtained, 2) the size of the cat brain lends itself to examination with small bore MR systems (4.7 and 9.4 T) capable of producing high-resolution signals, which can be then compared with histological results, and 3) adult cat brains have relatively complex gyral folding patterns and, therefore, provide closer comparison to monkeys and humans than do the brains of rats and mice.

Materials and Methods

Specimens

We performed scans on the brains of 2 newborn cats (P0), 2 kittens (P35), and 2 young adult cats (P70 and P100), obtained from a group involved in vision research. Although we scanned 2 brains at each developmental stage, we present in this article the data from one brain in each stage; this decision was made because one of the P0 brains was not in good condition. That particular P0 brain was incompletely fixed and fragmented, compared with the other one, possibly indicating that the brain was not properly perfused. As such, comparison between the diffusion properties of that brain and those of the perfused brain would have been compromised. The callosal connections of the P0 brain that we used were physically disconnected during craniotomy.

After the cats were euthanized, their brains were perfused with phosphate-buffered saline solution followed by 4% paraformaldehyde,

removed from the cranium, and fixed in 4% paraformaldehyde containing 1 mM gadolinium (Gd-DTPA) MRI contrast agent for 1 week to reduce the T_1 relaxation time while ensuring that enough T_2 -weighted signal remained. For MR image acquisition, the brains were placed in the Fomblin solution (Fomblin Profliudropolyether; Ausimont). We used 2 Bruker Biospec MR systems: a 9.4 T scanner for the 2 P0 specimens and a 4.7 T system for the other specimens.

Scanning Parameters

The pulse sequence used for image acquisition was a 3D diffusion-weighted spin-echo echo-planar imaging sequence, time repetition/time echo 1000/40 ms, with an imaging matrix of $112 \times 112 \times 128$ pixels for P0 brains, $96 \times 112 \times 128$ pixels for P35 brains, and $96 \times 96 \times 128$ pixels for P70 and P100 brains. Spatial resolution was $300 \times 300 \times 300 \mu\text{m}$ for the newborn kittens, $420 \times 420 \times 420 \mu\text{m}$ for the juvenile kittens, and $550 \times 550 \times 600 \mu\text{m}$ for the young adult cats. Anisotropic resolution may produce less spatial resolution along a longer axis compared with that along a shorter axis, which may mean that DSI tractography has less potential to resolve crossing pathways along the longer axis. However, the voxel size used for the young adult cats was nearly isotropic (less than 10% difference), and we believe it did not bias our tractography significantly.

We performed diffusion spectrum encoding as previously described (Wedeen et al. 2005). Briefly, we acquired 515 diffusion-weighted measurements, corresponding to a cubic lattice in q -space contained within the interior of a ball of maximum radius $b_{\text{max}} = 4 \times 10^4 \text{ s/mm}^2$, with $\delta = 12.0 \text{ ms}$, $\Delta = 24.2 \text{ ms}$. The total acquisition time was 18.5 h for each experiment.

Diffusion Data Analyses—DSI Reconstruction

DSI reconstruction was based on the Fourier relationship of the attenuated echo signal in q -space $E(q)$ and the average diffusion propagator of the water molecular diffusion $P_s(R)$:

$$E(q) = \int P_s(R, \Delta) \exp(i2\pi qR) dR,$$

where R is the relative displacement of water molecule diffusion during the diffusion time Δ . Based on this calculation, applying a 3D Fourier transform to the echo signal over the q -space would lead us to obtain the 3D probability density function (PDF) and then map the fiber orientations (Lin et al. 2003; Wedeen et al. 2005). The transformation from q -space signal to PDF values was performed voxel-by-voxel. To visualize the PDF, we integrated the second moment of PDF along each radial direction to acquire the orientation distribution function (ODF). In this study, we reconstructed the ODF within each voxel by interpolating along 181 radial directions, as calculated from the vertices of a regular and triangular mesh of the unit sphere surface. By comparing the length of each vector with the lengths of its neighboring vectors, we could obtain the orientational local maxima to represent intravoxel fiber orientations. We normalized all ODFs by the maximum ODF length within each voxel and calculated FA from orientation vectors by fitting the data to the usual tensor model.

Diffusion Data Analyses—Tractography

We used a streamline algorithm for diffusion tractography (Mori et al. 1999). Trajectories were propagated by consistently pursuing the orientation vector of least curvature. We terminated tracking when the angle between 2 consecutive orientation vectors was greater than the given threshold (35°) or when the fibers extended outside the brain surface, by using mask images of the brains created by MRicro (<http://cnl.web.arizona.edu/micro.htm>) for each specimen. In many tractography studies, FA values are used to terminate fibers in the gray matter, which in adults has lower FA values than the white matter. However, as one of the objectives of our study was to detect fibers in low FA areas, we used brain mask volumes to terminate tractography fibers without using the FA threshold for tractography. Trajectories were displayed on a 3D workstation (TrackVis, <http://trackvis.org>). The color coding of fibers is based on a standard RGB code, applied to the vector between the end points of each fiber.

Filtering for Tractography

For visualization purposes in the figures, we restricted the percentages of the number of detected tractography pathways in the following

ways. In Figure 1 (C, D) and Figure 2 (C), we omitted tractography fibers less than 2 mm long to ensure that we were identifying coherent tracts over at least 6 voxels. This reduced the likelihood that noise in low FA areas was driving our results. Figure 2B shows 50% of the fibers that touched a coronal slice with thickness of 10 voxels. Figures 3D and 4C,D show 10% of the fibers that touched each coronal slice. Figure 5 shows all tractography pathways longer than 2 mm.

Histology—Thionin (for Cell Bodies)

After MRI scanning, the brains were soaked in sucrose solutions (10% and then 30%), frozen, and sectioned at 40 μ m. After being left in distilled water for 3 min, the slides were soaked in thionin solution for 5 min, followed by distilled water for 30 s, 95% ethyl alcohol for 10 s, 100% ethyl alcohol for 2 \times 3 min, and finally in xylene 2 \times 5 min and mounted with resinous medium. As a result of this staining process, neuronal cell bodies appear violet in color.

Histology—Luxol Fast Blue (for Myelinated Fibers) Counterstained with Cresyl Violet (for Cell Bodies)

After MRI scanning, brains were soaked in sucrose solutions (10% and then 30%), frozen, and sectioned at 40 μ m. After a defatting step, in which the slides were soaked in 1:1 alcohol/chloroform for a few hours and then rehydrated with 95% ethyl alcohol, they were left in Luxol Fast Blue solution in a 56°C oven overnight (14 h). After a rinse with 95% ethyl alcohol and distilled water to remove excess stain, the slides were differentiated in lithium carbonate solution for 30 s and then in 70% ethyl alcohol for 30 s. The slides were then rinsed in distilled water. We checked under a microscope to determine that the gray matter was clear and white matter sharply defined. This step was especially important in the P100 brain as there are abundant examples in the literature showing that myelination is significantly progressed at P100. We used the same procedure for the P0 and P35 brains. Next, the slides were counterstained in Cresyl Violet solution for 30–40 s. After a rinse in distilled water, the slides were differentiated in 95% ethyl alcohol for 5 min, in 100% alcohol 2 \times 5 min, and finally in xylene 2 \times 5

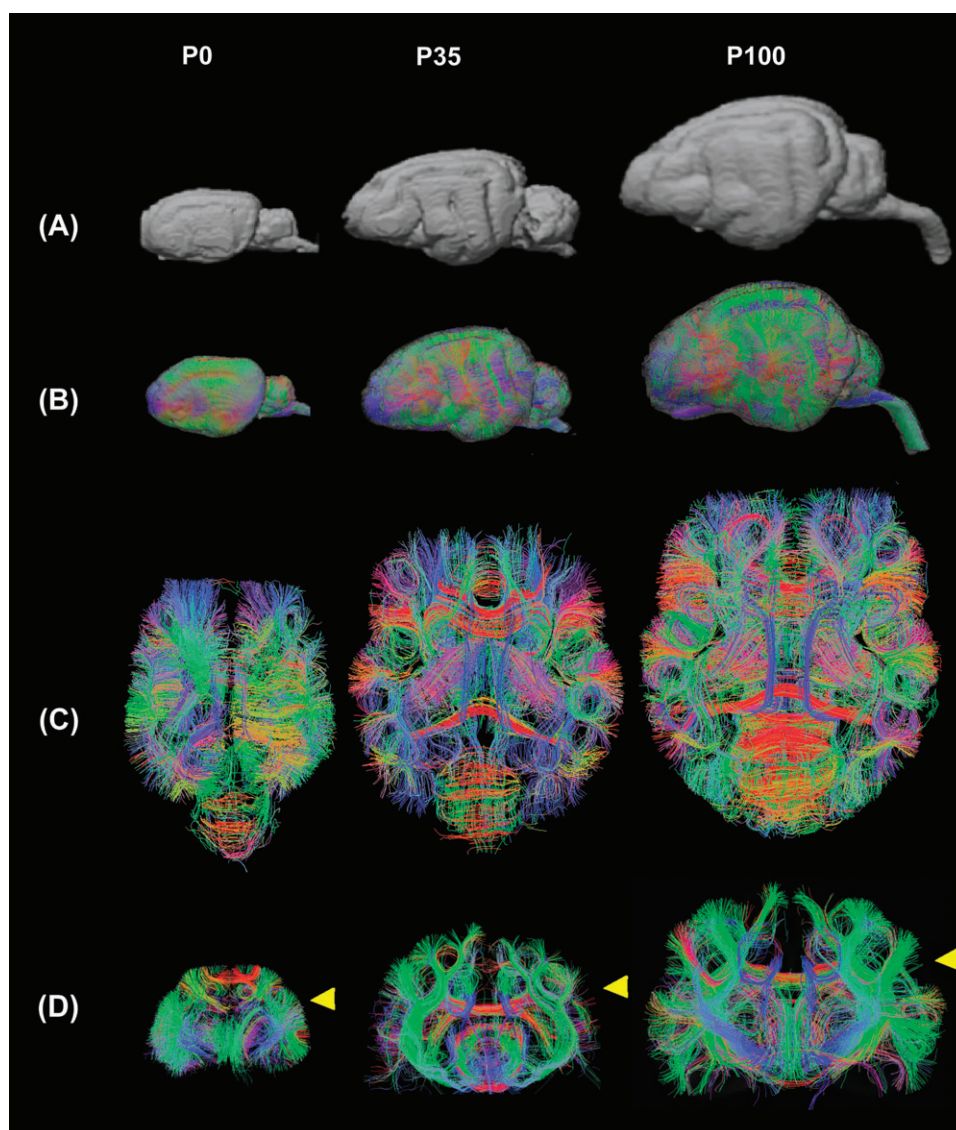


Figure 1. (A) Gyral patterns of 3 time points, (B) whole-brain DSI tractography, (C) axial, and (D) coronal slices of the whole-brain DSI tractography at P0, P35, and P100. With age, the structural organization became less uniform; as gyral formation increased, there was increasing prominence and regional variation of intra- and intercortical pathways. The left side of the image represents the anterior side of the brain in (A) and (B) and the left side of the brain in (C). Colors indicate spatial relationships between fiber end points. Red: left–right, blue: anterior–posterior, and green: dorsal–ventral orientation. Yellow arrows in (D) indicate slice levels of panel (C). As we explain in greater detail in the text, callosal connections in the P0 brain were disconnected at the midline during craniotomy, so in the P0 brain, callosal tractography pathways appeared in green (dorsoventral direction: from the corpus callosum to the cortex).

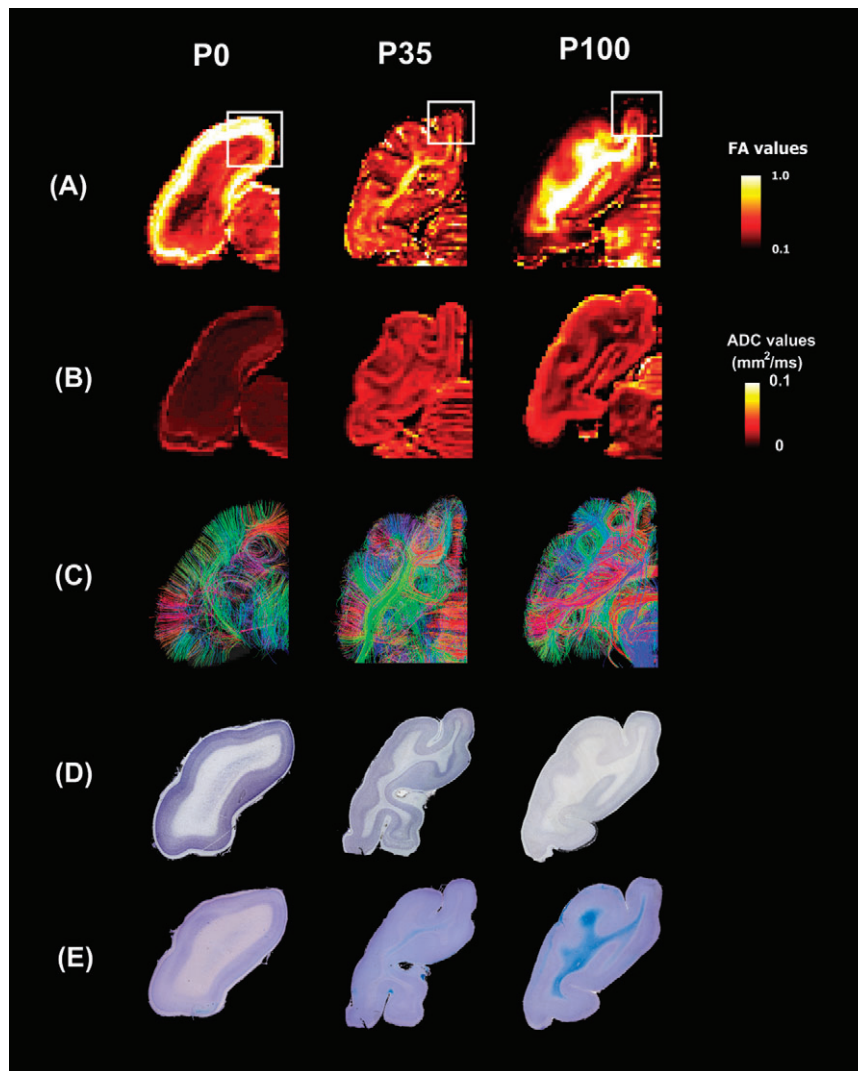


Figure 2. FA maps (A), ADC maps (B), diffusion tractography pathways (C), thionin stainings (D), and Luxol Fast Blue counterstained with Cresyl Violet stainings (E). The P0 brain showed the highest FA values in the CP and immediately adjacent SP. For magnified view, see Figures 3 and 4. They are all coronal sections that included the primary visual areas on the dorsal surface of the brain. The maps were from individual cat brains of P0 (left column), P35 (middle column), and P100 (right column). The color scale indicates FA values in (A) and ADC values in (B). Left side of the image represents left side of the brain. (C) Colors indicate spatial relationships between fiber end points. Red: left–right, blue: anterior–posterior, and green: dorsal–ventral orientation. Panels (A) and (E) were reused (license number: 2362120782942 provided by Elsevier 2010).

min and mounted with resinous medium. As a result of these staining procedures, myelin including phospholipids is stained blue, and neuronal cell bodies are stained pink to violet.

Registration of Histology and Tractography

We selected corresponding slices from the histology and DSI tractography data based on the length from the posterior edge of the brain (3.0 mm for the P0 brain, 5.0 mm for the P35 brain, and 7.0 mm for the P100 brain, from the posterior edge of the brain surface, which corresponds to the middle of the primary visual cortex) and adjusted scales for both data sets. We then overlaid the 2 types of images by defining 3 reference points and using those points to rotate the tractography images until the maximum number of terminal points fell on the edge of the brain surface, using ImageJ software (<http://rsbweb.nih.gov/ij/>). We tried to minimize the registration errors by this approach since we terminated tractography pathways at the edge of the brain surface, by using mask images as noted above in “Diffusion Data Analyses—Tractography.”

We marked the approximate layer boundaries (Figs 3 and 4) based on available literature (Friauf et al. 1990; Ghosh and Shatz 1993). Note that we do not mark layers based on the FA maps as we show here at least in

the CP and SP that high FA does not identify the CP but the CP and outer SP.

Comparison of Developmental Stages between Cats and Humans

Although it is not possible to directly compare developmental stages between different species, we have estimated the equivalent developmental stages of cats and humans based on the starting periods of gyral formation, existence of the SP and the CP, and penetration of the thalamocortical fibers into the CP (Issa et al. 1999; Kostovic and Jovanov-Milosevic 2006; Kostovic and Vasung 2009). Issa et al. (1999) compares development of cats and ferrets, and Kostovic and colleagues have summarized human fetal development.

Results

Whole-Brain DSI Tractography

Whole-brain DSI tractography fibers were detected at all ages as the gyral structure developed (Fig. 1A,B). Axial (Fig. 1C) and coronal (Fig. 1D) slices of the whole-brain DSI tractography

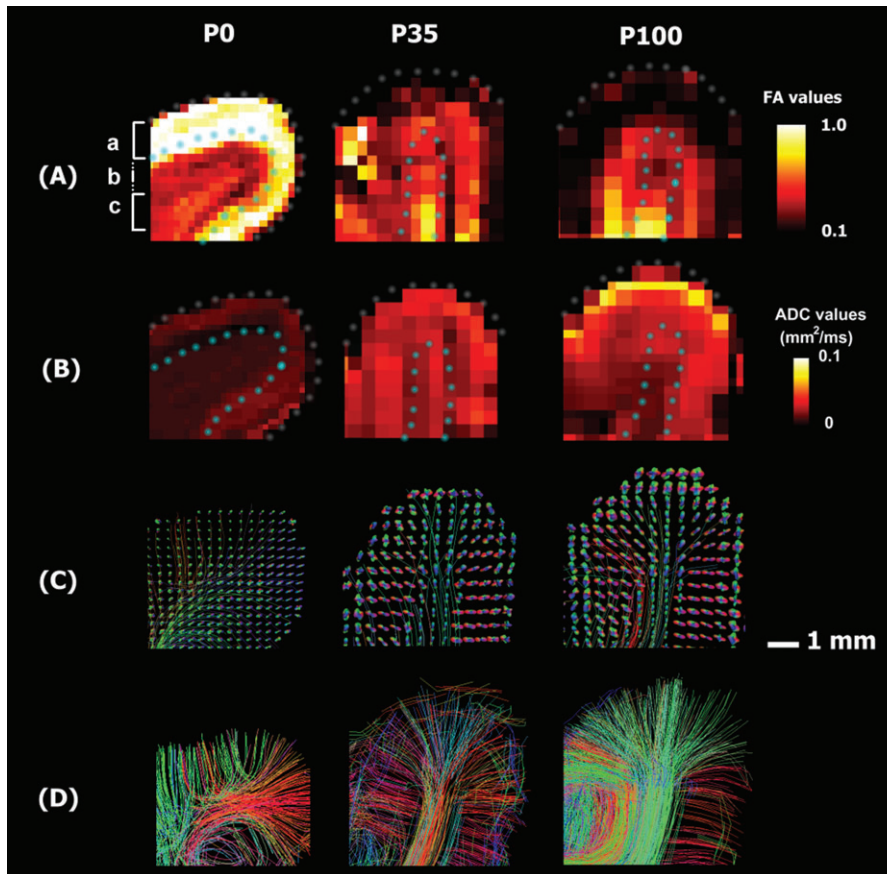


Figure 3. Magnified images of FA maps (A), ADC maps (B), ODFs with representative tractography pathways (C), and tractography pathways passing through the coronal plane (D). Areas with high FA values were found extended beyond the CP into the adjacent outer SP. FA values in the cortex became more variable and globally decreased at P35 with a poorly defined difference between cortex and underlying white matter. Tractography pathways were detected not only in high FA areas but also in low FA areas. The color scale indicates FA (A) and ADC (B) values. Approximate borders of the brain surfaces and the white/gray matter borders were shown in dotted lines in (A) and (B). The scale bar indicates 1 mm. Left side of the image represents left side of the brain. Colors of tractography fibers indicate spatial relationships between fiber end points. Red: left-right, blue: anterior-posterior, and green: dorsal-ventral orientation. (a) CP, (b) SP, and (c) IZ.

showed increasing regional variation with age. The P0 brain was much more uniform in structure. With age, the structural organization became less uniform; as gyral formation increased, there was increasing prominence and regional variation of intra and intercortical pathways.

Comparisons of Diffusion Measures and Histology in Global and Finer Scales

We compared FA maps (Fig. 2A), ADC maps (Fig. 2B), diffusion tractography pathways (Fig. 2C), thionin stainings (Fig. 2D), and Luxol Fast Blue counterstained with Cresyl Violet stain (Fig. 2E). All sections were coronal and included the primary visual cortex on the dorsal surface of the brain.

We next magnified areas corresponding to those outlined by white rectangles in Figure 2A and compared diffusion/histological measures in those areas. Figure 3 includes maps of FA (Fig. 3A), ADC (Fig. 3B), ODF with some representative tractography pathways (Fig. 3C and Supplementary Figs S1–S3), tractography pathways passing through a cortical slice (Fig. 3D), thionin staining (Fig. 4A), Luxol Fast Blue counterstained with Cresyl Violet (Fig. 4B), tractography pathways shown in Figure 3D superimposed on the slices of thionin staining (Fig. 4C), and the same tractography pathways superimposed on the FA maps (Fig. 4D).

FA Values and Correlation of FA and Thionin and Luxol Fast Blue/Cresyl Violet Stains

The P0 brain showed the highest FA values in the CP and immediately adjacent SP. The thickness of the CP was uniform at P0 with thionin staining for cell bodies revealing a dense cellular and radial cortical organization. Coregistering thionin-stained sections to FA maps showed high FA values extending beyond the CP (1 mm in the P0 brain) approximately 0.5 mm into the adjacent outer SP (Figs 3A and 4), where there was a sharp transition to lower FA. Then with increasing distance away from the CP, FA values rapidly decreased with a small increase in FA noted in the deepest areas of the white matter, corresponding to the expected location of the IZ (Figs 2A,E, 3A, and 7).

The P35 brain had lower FA values in the cortex than the P0 brain, with associated increased regional variation in cortical FA. The highest FA values were observed in the deep white matter, where greater myelination was observed (Figs 2A,E, 3A, and 7). FA values in the P100 brain (Figs 2A, 3A, and 7) were even lower and more uniform in the cortex than at P35, with a more rapid transition at the gray-white matter boundary to increased FA in the subcortical white matter (2 mm from cortical surface). In the P35 and P100 brains, cortical thickness became more variable, with thionin staining revealing

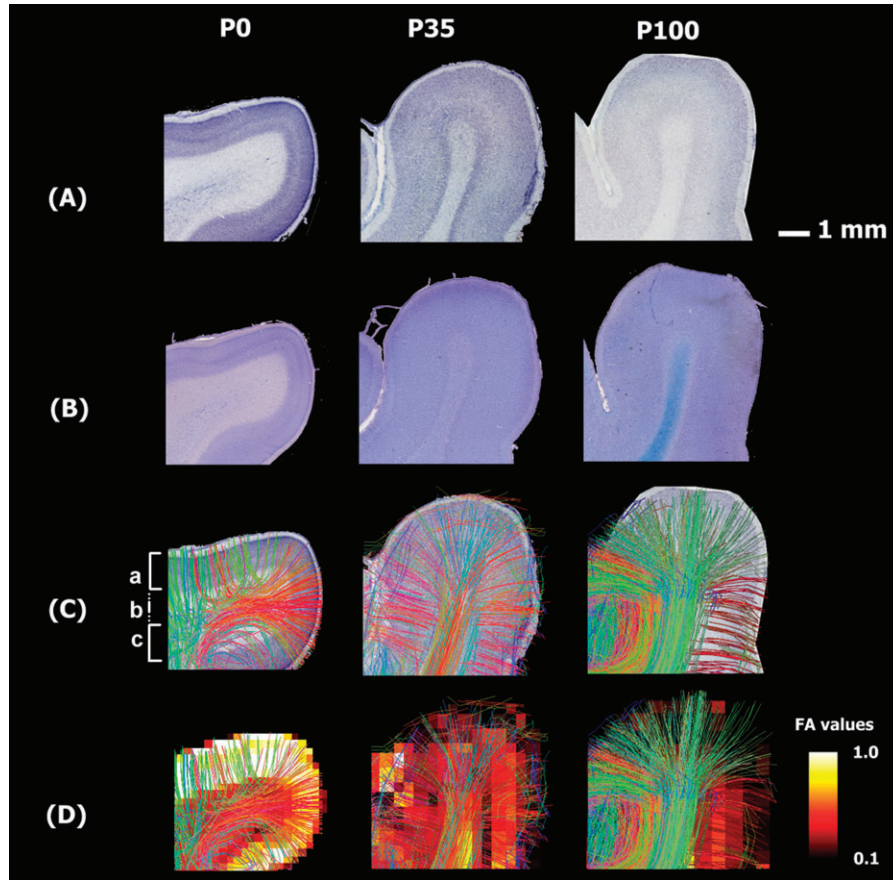


Figure 4. Magnified images of thionin staining (A), Luxol Fast Blue /Cresyl Violet stainings (B), tractography pathways superimposed onto the thionin staining (C), and tractography pathways superimposed on the FA map (D) of P0 (left column), P35 (middle column), and P100 (right column) brains. In the P0 brain, the CP and outer SP had radial coherent fiber pathways corresponding to regions of high FA, while the inner SP with low FA contained abundant crossing pathways. In the expected location of the IZ pathways became more coherent and crossed at smaller angles. In contrast, more white matter compartmentalization was visible at P35 and P100 in the white matter. The color scale indicates FA (D) values. The scale bar indicates 1 mm. Left side of the image represents left side of the brain. Colors of tractography fibers indicate spatial relationships between fiber end points. Red: left-right, blue: anterior-posterior, and green: dorsal-ventral orientation. (a) CP, (b) SP, and (c) IZ.

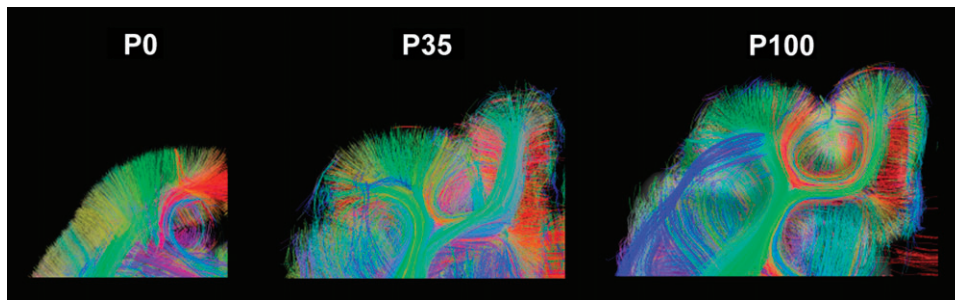


Figure 5. All tractography pathways longer than 2 mm passing through the illustrated coronal slices. Left side of the image represents left side of the brain. Colors of tractography fibers indicate spatial relationships between fiber end points. Red: left-right, blue: anterior-posterior, and green: dorsal-ventral orientation.

decreasing cellular density but persistent radial cortical organization. FA values in the cortex also became more variable and globally decreased at P35 with a poorly defined difference between cortex and underlying white matter.

In the P0 brain, there was no clear myelin staining by Luxol Fast Blue; in the P35 brain, there was weak myelin staining in the deep white matter, and in the P100 brain, the white matter was strongly stained throughout, appearing deep blue (Fig. 2E). In areas of myelin staining at P100, FA values continued to gradually increase with greater distance from the pia, with the highest values in the deep white matter (Figs 2A,E and 3A). This

increased staining with age was consistent across multiple sections and was comparable in location to the regions of white matter with high FA in the P35 and P100 cats (Fig. 2A). There was no significant intracortical myelin staining in the cortex at any age. Cresyl Violet stains (Fig. 2E, appearing in violet) revealed a laminar and radial cortical organization in all ages, as with thionin staining.

ADC Values

ADC maps (Figs 2B and 3B) showed overall lowest values in the P0 brain compared with P35 and P100 brains, probably

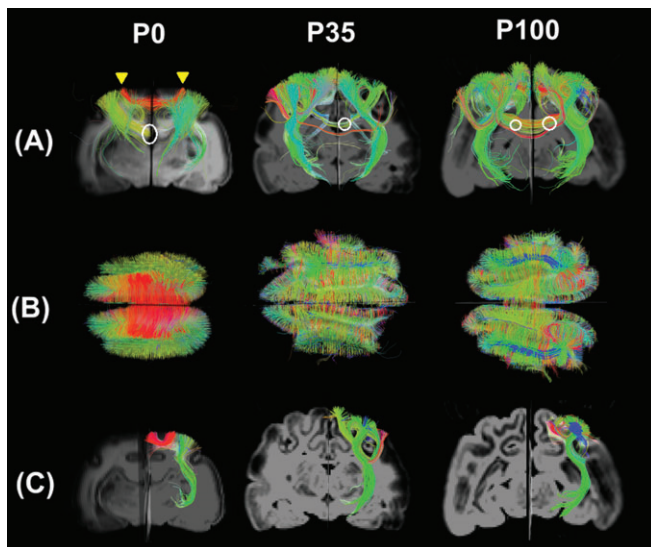


Figure 6. Coronal (A) and axial (B) views of fibers running through a coronal (A) and an axial (B) slice. (C) Examples of intrahemispheric short (red in P0) and long association fibers (blue in P35 and P100) and thalamocortical fibers (green) in P0 (left column), P35 (middle column), and P100 (right column) brains. Intrahemispheric tractography fibers running between visual areas 17 and 18 (yellow arrows in panel A) are most prominent at P0 compared with P35 and P100, whereas long association fibers (for example pathways in blue in panels A and B) become more prominent at P35 and P100 compared with P0. Colors indicate spatial relationships between fiber end points. Red: left–right, blue: anterior–posterior, and green: dorsal–ventral orientation. The white circle in (A) at P0 represents areas where callosal connections were disconnected due to craniotomy. Although callosal fibers fully exist at P35 and P100, some fibers appear to be disconnected due to fiber reconstruction and the appearance of the cingulum bundle, which runs perpendicular to the callosal fibers. The white circles at P35 and P100 designate the area of intersection of these bundles. These resulted in showing some green fibers as the callosal connection. For an example of magnified image, see Supplementary Figure S7. Left side of the image represents left side of the brain in (A) and (C). In (B), upper side of the image represents anterior side of the brain.

resulting from differential fixation, as will be discussed later. In the P0 brain, ADC values were higher in the 1-mm outer margin, with a rapid transition to lower values in the white matter (Figs 2B, 3B, and 7). The region of higher ADC matched well to the CP, revealed by thionin staining (Figs 2 and 4), with the immediately adjacent SP having lower ADC despite similar high FA values to CP (Figs 2A, 3A, and 7). ADC maps of the P35 brains also showed higher ADC values in the cortex, with a rapid transition to lower ADC values in the subcortical white matter and a continued gradual decrease to the deepest white matter (Figs 2B, 3B, and 7). The deepest white matter that showed the lowest ADC values included the areas with high FA and myelin staining (Fig. 2B,E), and low ADC areas also extended into the more superficial unmyelinated areas. However, some unmyelinated areas showed high ADC. There was no clear pattern that correlated unmyelinated areas and high ADC areas. Therefore, at P35, FA values correlated better with the degree of myelination than with ADC values.

ADC maps of the P100 brains again showed higher ADC values in the cortex, with a sharper transition to even lower ADC values in the subcortical white matter, and only a small additional decrease in the deepest white matter (Figs 2B and 3B, right). The less than 0.5 mm of unmyelinated subcortical white matter in P100 could not be adequately resolved from the adjacent cortex and myelinated white matter at the resolution of this study.

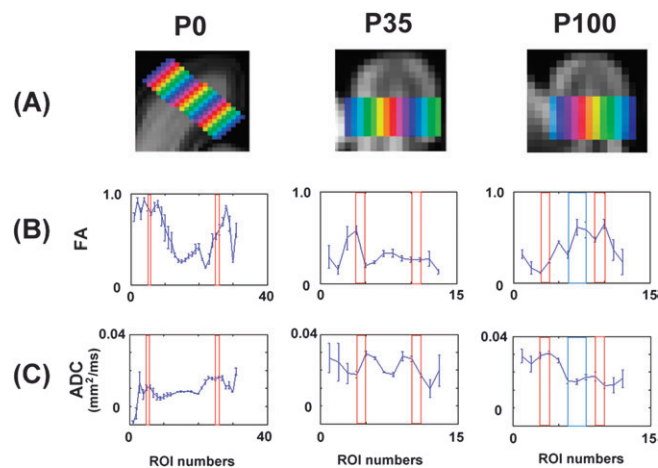


Figure 7. Region of interest (ROI) analysis of cortex. (A) Sequential ROIs placed horizontally from one brain surface to the other in P0 (left), P35 (middle), and P100 (right) brains. (B,C) Plots of FA (B) and ADC (C) values across the ROIs. *x*-Axis represents ROI numbers corresponding to each one from one brain surface to the other (middle area represents deep white matter). The white/gray matter borders were shown as red rectangles, and the area stained by Luxol Fast Blue (myelin stain) is shown as blue rectangles at P100.

Tractography

Figures 2C, 3D, 4C,D, and 5 show tractography pathways passing through the illustrated coronal slices. The deep white matter had pathways running parallel to the pial surface in the P0 brain, which appeared to contain long projection tracts localized to the expected region of the IZ. In the inner SP, these pathways curved sharply, crossed with other intrahemispheric pathways, became radially oriented in the outer SP, and remained radial as they entered the CP (Fig. 2C, left). Therefore, the deeper SP contained many crossing pathways, whereas the outer SP was highly radial (see also Fig. 5). In the P35 and P100 brains, we also observed coherent fiber pathways in the deep white matter that curved rapidly outward to enter the cortex radially (Fig. 2C, middle, right). We also observed local horizontal fiber pathways within the cortex that may reflect forming horizontal interneuron connections at P35 and P100 (Fig. 3D). In the P35 and P100 brains, regions rich in crossing pathways, as in the inner SP at P0, were not uniformly observed but became more restricted to specific gyri containing long association pathways (Fig. 5). At P35 and P100, fibers in gyri also became more compartmentalized, with subcortical U-fibers at the periphery of the gyrus and longer-range projection pathways located more centrally. In some regions perpendicular to the projecting pathways, long association fibers were also identified. This regional variation became more prominent from P35 to P100.

Comparisons of Tractography Pathways, Histology and FA Maps in a Finer Scale

We compared tractography fibers with slices of thionin staining and FA maps (Fig. 4A–D and Supplementary Figs S4–S6) from these areas, by coregistering tractography pathways with the thionin staining and FA maps. In the P0 brain, the CP and outer SP had radial coherent fiber pathways corresponding to regions of high FA, while the inner SP with low FA contained abundant crossing pathways (Fig. 4C, left). In the expected location of the IZ pathways became more coherent and crossed at smaller

angles. Thus, many of the radial pathways in the CP and outer SP passed through the inner SP with low FA as they connected with pathways of diverse directions. In contrast, more white matter compartmentalization was visible at P35 and P100, with individual gyri having coherent projection pathways emerging/entering centrally, and longer-range association pathways being increasingly evident. These association pathways crossed perpendicularly to long-projection pathways in the central white matter of the gyrus (Fig. 5). In the P35 and P100 brains, the thickness of the cortex (around 1.5 mm in the P35 and around 2 mm in the P100 brains) corresponded to the highly radial pathways on DSI despite the low FA values (Fig. 4D).

DSI Tractography—Connections between Visual Areas 17 and 18 and Callosal Connections

Following observations of exuberant connectivity in the developing visual cortex (Innocenti and Price 2005), we looked for supportive evidence in the images. Figure 6 shows coronal (Fig. 6A) and axial (Fig. 6B) views of fibers passing through an axial slice close to the visual areas. Pathways shown in Figure 6A are further filtered by a coronal slice for visualization purposes. Intra-hemispheric tractography fibers running between visual areas 17 and 18 (Fig. 6B,C in red) are most prominent at P0 compared with P35 and P100, whereas long association fibers (e.g., Fig. 6B,C in blue) become more prominent at P35 and P100 compared with P0.

Callosal connections (Fig. 6A) can be seen coursing between the 2 hemispheres at P35 and P100. However, in the P0 brain, all callosal fibers are physically disconnected in the midline during the craniotomy, so they are light green because in each hemisphere the callosal fibers run approximately in a dorsal-ventral as well as left-right directions toward midline. The image of the P0 brain (Fig. 6A) clearly shows that the callosal fibers are disconnected in the middle. The reason these green fibers also exist in P35 and P100 brains is that there are some disconnected fibers around the midline (not physically, but during tractography reconstruction) due to the partial volume effect from the adjacent cingulum bundle. However, there are also many red fibers running in the left-right direction (see Supplementary Fig. S7).

Discussion

In this report, we present the first DSI tractography study focused on the CP/cortex and SP/subcortical white matter with histological correlation of the P0, P35, and P100 cat brain. The CP at P0 as well as the cortex at P35 and P100, is dominated by a highly radial organization that appears to result from the persistent radial organization of neuronal columns along with efferent/afferent axonal pathways. At P0, the outer SP is also highly radial, probably due to radially oriented SP neurons in addition to the efferent/afferent axonal pathways. At P0, radial glial fibers are unlikely to play a major role as no radial structures spanning the whole of the cerebral mantle were observed. The deeper SP zone contained multiple crossing interhemispheric and intra-hemispheric pathways, which resulted in low FA. At P35 and P100, in the presence of gyral folding, the organization of the white matter appeared more compartmentalized, and more compact long range association fibers appeared. These results agree with the known decrease in interhemispheric corpus callosum connections between visual areas with maturation and with

the increase in ipsilateral corticocortical connections. Our results show the usefulness of DSI in fixed pathological specimens, irrespective of the degree of myelination, for providing information on developing cortical structure and connectivity.

Maturation of Cortical Organization That May Affect Diffusion Imaging Measurements

In early developmental stages, the immature cortex (CP) begins to be prominent around W15 in humans (for review, Kostovic and Jovanov-Milosevic 2006) and around E26 in the cat (Luskin and Shatz 1985). Following the formation of the CP, a large contingent of pyramidal neurons migrates radially, along radial glia, from the ventricular germinal zone to the CP. These neurons arrive at their final destinations in the fetal CP and organize into radially oriented, inside-out columns (Sidman and Rakic 1973). On the other hand, thalamic neurons elongate their axons parallel to the brain surface along the layer interposed between the subventricular zone and the CP—the IZ—and terminally grow into the CP toward appropriate target neurons (Ghosh and Shatz 1992). Coincident with and following the migration processes, maturation of the CP occurs. At birth, a radial organization is still present in the cat and persists until at least P30, although it is less prominent compared with earlier stages of development (Engel and Muller 1989). Such developmental changes in cellular morphology modify the developing CP from a dense cellular radial organization with minimal regional specification to a mature, less radial organization showing decreased cellular density and increased dendritic arborizations.

Although white matter tract development has been studied using FA or ADC measures (Huppi et al. 1998; Neil et al. 1998; Mori et al. 2001; Miller et al. 2002), the changes in water diffusivity in the developing cortex have been less explored. FA values in the CP have been reported to be high and to decrease with maturation of the cortex (McKinstry et al. 2002). There are several developmental events that may influence water diffusion in the cortex during postnatal cortical development, which may be responsible for the decrease in water diffusion and anisotropy that we observed. These include 1) expansion of dendritic trees (Marin-Padilla 1992), 2) formation of horizontal connections (Callaway and Katz 1990), 3) eliminations of selected cell populations (Sidman and Rakic 1973), and 4) increased ramification of oligodendrocytes (Rivkin et al. 1995; Hardy and Friedrich 1996). However, despite the decrease in cortical FA, we show that a dominant radial organization persists throughout all developmental stages, most likely reflecting the presence of radially oriented neurons as well as afferent and efferent axons. In the developmental stages studied here, it is unlikely that the radial glial fibers contribute to this radial tractography pathways, given that there no radial pathways were observed extending from the ventricular wall to the CP. Future histological studies aimed on outlining the axons in the area will be necessary to further identify the origin of the signals that result in our tractography results in this area of the cortex at this stage.

In the cat, cortical horizontal connections begin developing just after birth (Callaway and Katz 1990), which corresponds to around W25 in the human. The results of the present study, which show significantly reduced FA values in the cortex P35 and P100 compared with P0 (Fig. 3), are consistent with this

earlier finding. Similar observations have been made in the developing brains of other animal species (Baratti et al. 1999; Mori et al. 2001; Kroenke et al. 2005, 2007) and in humans (Kostovic et al. 2002; McKinstry et al. 2002; Maas et al. 2004), whereby the corresponding stage of horizontal fiber development occurs between prenatal W26 and W35.

The SP has been reported to be an area with very low FA values, in contrast with the adjacent CP, which has higher FA values (highly anisotropic until W32, for review, see Prayer et al. 2001). However, due to the low imaging resolution and lack of histological correlation of previous studies, the detailed structure of the boundary region between the CP and the outer SP has not been visualized clearly. On the other hand, our present results show relatively high FA extending in the external portion of the SP and low FA immediately deeper. In the SP area, we attributed the low FA values of the deep SP to the presence of many crossing fibers. Thus, more than 1 mm from the inner margin of the CP, ODFs typically showed multiple peaks, likely corresponding to crossing fibers in the SP. This suggests that the SP should more accurately be divided into an outer highly radial structure dominated by radially oriented SP neurons and an inner zone rich with crossing efferent and afferent connections. However, this conclusion may not be entirely correct since the SP, especially the outer SP, also contains a many nonaxonal cellular elements, which could influence the local diffusion properties and lead to local anisotropy that can be interpreted as fiber trajectories (e.g., Kostovic and Jovanov-Milosevic 2006).

White Matter Development That May Affect Diffusion Properties and Tractography

In the current study, myelin in the white matter was stained by Luxol Fast Blue: strongly in the brains of P100 cats and relatively weakly in the P35 brains; no significant staining was observed in the P0 brains. Myelination in the human brain is a long process that starts before birth and continues through adulthood (Flechsig 1920), with maturation of the motor and sensory tracts preceding that of the corticocortical association fibers, which in turn precedes the myelination of intracortical fibers (Yakovlev and Lecours 1967; Brody et al. 1987). Cortical myelination remains active into senescence (Yakovlev and Lecours 1967; Brody et al. 1987). However, the majority of myelination is complete by 2 years and similarly most parts of the human brain show an increase in FA values (approximating adult values) by 2 years of age (Schmithorst et al. 2002; Zhang et al. 2005). The onset of myelination in the brain varies in different fiber tracts and species, but on average, starts around E40 in the spinal cord and around P20 in the callosal areas in the cat (Remahl and Hildebrand 1982, 1990); therefore, it is likely that myelination occurs in the thalamocortical tracts sometime between E40 and P20 in the cat. This presumed time frame for myelination would agree with our FA mapping (Figs 2A and 3A) and histology (Figs 2G and 4B) results, which showed gradual increase in FA values in the white matter and stronger LFB staining during development. The deep white matter where we observed weak myelination at P35 largely corresponded to corticospinal and thalamocortical fiber pathways. The reason why we did not observe myelin staining at P0 was due in part to the lesser degree of myelination at that stage of development, but also at the relatively high threshold for visualization of myelin with the LFB technique.

The density of axonal connections is greater at birth than in the adult (for review, Innocenti and Price 2005). As unused fibers are pruned and the volume and length increases, the density of axonal connections decreases. Tract volume increases are primarily due to progressive myelination. At the same time, myelination also causes high diffusion coherency in the white matter enabling easier tractography reconstruction. These factors (increasing tract myelination, volume, and length) contribute to finding more tractography fibers even though there are fewer axons present. This is a reconstruction artifact effecting visual perceptions that researchers need to be aware of when interpreting tractography studies.

Postperfusion Processes and Scanning Conditions That May Affect Diffusion Imaging Measurements

Diffusion imaging of the postmortem brain allows us to acquire very high-resolution results from a long-duration experiment, but at the same time, fixation processes used on the post-mortem brain tissue changes the diffusion properties (FA/ADC) compared with those observed in vivo (D'Arceuil and de Crespigny 2007; Dawe et al. 2009). Thus, comparing such high-resolution tractography and FA/ADC is very important for interpreting the results from this direction of research on the postmortem brain and for aiding future efforts to further improve the technique.

Although living fetal and infant brains show ADC values that are higher than those in adults (Hermoye et al. 2006), ADC values in the ex vivo specimens are variable. In this study, we observed lower ADC values in the P0 brain after fixation. In a previous study, the fixation processes resulted in an overall greater shrinkage of fetal brains compared with adult brains, with the fetal brains shrinking approximately 75%, plus or minus 20% (Kretschmann et al. 1986). Such a degree of shrinkage could cause low ADC values, as explained by a reduction in the extent of water diffusion in both intra- and intercellular spaces. However, the thickness of the cortex in the P0 brain in this study was comparable to that reported in the literature (Innocenti and Price 2005), indicating that our specimen did not undergo excessive shrinkage. Others have reported that fetal brains fixed in paraformaldehyde acquire water (McLennan et al. 1983), but it is unclear whether the protein cross-linking caused by the fixative results in overall lower ADC values in less dense, unmyelinated regions where paraformaldehyde is likely to accumulate. Because of the variable and unpredictable effect of fixation on ADC values, absolute values of ADC in fixed specimens cannot be easily compared among different ages.

It may also be possible that potential differences between the MRI gradient systems on the 4.7 and 9.4 T magnets could result in systematic differences in ADC value. However, it would be reasonable to assume that a stronger gradient system would cause larger diffusivity, and future systematic examination is needed to properly assess the meanings of ADC measures in the fixed immature brains.

Registration Issues

We tried to register the MRI and histology images as precisely as possible. However, the angles of the slices are slightly different, especially in the P35 brain, and registration was not perfect, especially for the second gyrus from the midline. The different slice thickness of MRI (400 μm) and histology (40 μm)

is another factor that makes registration challenging. In other words, MRI slices contain an average of about 10 histology slices. However, given that we focused mainly on the first gyrus from the midline to directly correlate MRI and histology, and our conclusions could be verified by comparison of the P0 and P100 brains, we anticipate that these issues have relatively small effect on our conclusions.

The reasons why the tractography pathways extended outside the brain around 100 μm in those figures are as follows. First, the pathways outside the brain could be due to the MRI signal from a slice adjacent to the shown histological slice because of the difference in slice thickness explained above. Second, in addition to different thicknesses, the angles of MRI and histology slices are slightly different, so registration is not 100% perfect. Third, it is known that the surface between different materials (in this case, between the solution and the brain) can easily cause artifact or noise around the surface. Although we have used the Fomblin solution to reduce susceptibility artifact, we indeed observed some ODFs with multiple peaks at the very surface of the brain (Supplementary Figs S1–S3), which could have caused errors in tractography at the surface of the brain. In that case, tractography data for layer I could have also been affected by artifact. There is a method to mask out the tractography results using the histology slice, which is sometimes used in MRI studies. However, we preferred to show the original results as they are, while providing explanations as above.

Conclusions—Linking between MRI and Histology

Using DSI, a uniform highly radial CP and outer SP was observed in the P0 (newborn) kitten and is likely due to the dense radial cellular organization of the CP in combination with afferent and efferent connections that enter/exit the CP. Although the etiology of the high radial organization of the outer SP was not determined in this study, we postulate that it is due to radial SP neuron projections that extend into the CP. The radial organization of the cortex persisted in the P35 (pediatric) and P100 (adult) cats, although it became less pronounced and more regionally variable with age. The inner SP was rich with abundant crossing pathways with little regional variation. After the SP disappeared, the white matter became more compartmentalized with long-range association pathways emerging and local intrahemispheric connections decreasing.

Unlike histological measures, MRI does not provide direct evidence of the existence of fiber pathways or neuronal components. Examination of postmortem brains for many hours using a high-field MRI scanner allows us to see “very high-resolution” water diffusion from which we can infer coherent fiber pathways, but we are still not able to directly distinguish which tractography pathways represent axons, glial fibers, or aligned cell components. DSI also has limitations in the detection of incoherent fibers or small fiber bundles. In particular, the horizontal intracortical organization is difficult to detect. We admit that this limitation is part of the nature of current MRI studies and that histology is superior to MRI in terms of resolution and directness. However, as we have explained in the introduction, histology has a different type of limitation, which precludes study of global fiber connections. One of the main contributions of our current work to these two fields has been direct correlation of “high-resolution” MRI and histology to determine what tractography can detect, to

what extent. This is a very important and necessary step (Kier et al. 2004) toward applying tractography in future clinical studies in vivo, and the current limitation of our technique does not necessarily decrease the significance of our study itself.

We still tend to miss tangential connections in the cortex, but in this study, we were able to detect these pathways in the P35 cortex, possibly because the FA values in the cortex at P35 were not as high as at P0 and not as low as at P100. The ODF had multiple resolvable peaks in the cortex at P35, which allowed us to track fibers in the tangential direction. We have explained this in the discussion section. Improved detection of tangential cortical connections is a strong interest of ours and we are exploring a number of different diffusion acquisition and postprocessing approaches to improve their detection.

Although the density of radial glial fibers needed to detect their presence as tractography pathways is not yet defined, we believe our data provide new information on early brain development. More detailed correlation between histology and imaging is certainly needed to understand more fully the limitations of both techniques, and such studies are currently underway. The ultimate goal is to be able to apply ex vivo animal approaches to in vivo human studies but we believe that high-resolution imaging studies with detailed histological comparisons are necessary to provide a solid foundation for in vivo interpretation.

Supplementary Material

Supplementary Figures S1–S7 can be found at: <http://www.cercor.oxfordjournals.org/>

Funding

NIH (RO1 MH 64044); National Science Foundation (PHY 0855161, PHY 0855453), and the Ellison Medical Foundation (208556).

Notes

We appreciate Veronica Peschansky for technical support and Danielle D. Sliva and Nichole Eusemann for editorial comments. *Conflict of Interest:* None declared.

References

- Allendoerfer KL, Shatz CJ. 1994. The subplate, a transient neocortical structure: its role in the development of connections between thalamus and cortex. *Annu Rev Neurosci.* 17:185–218.
- Baratti C, Barnett AS, Pierpaoli C. 1999. Comparative MR imaging study of brain maturation in kittens with T1, T2, and the trace of the diffusion tensor. *Radiology.* 210:133–142.
- Barkovich AJ, Kjos BO, Jackson DE Jr, Norman D. 1988. Normal maturation of the neonatal and infant brain: MR imaging at 1.5 T. *Radiology.* 166:173–180.
- Basser PJ, Mattiello J, LeBihan D. 1994. Estimation of the effective self-diffusion tensor from the NMR spin echo. *J Magn Reson B.* 103:247–254.
- Basser PJ, Pajevic S, Pierpaoli C, Duda J, Aldroubi A. 2000. In vivo fiber tractography using DT-MRI data. *Magn Reson Med.* 44:625–632.
- Brody BA, Kinney HC, Kloman AS, Gilles FH. 1987. Sequence of central nervous system myelination in human infancy. I. An autopsy study of myelination. *J Neuropathol Exp Neurol.* 46:283–301.

- Callaway EM, Katz LC. 1990. Emergence and refinement of clustered horizontal connections in cat striate cortex. *J Neurosci*. 10:1134-1153.
- Cellerini M, Konze A, Caracchini G, Santoni M, Dal Pozzo G. 1997. Magnetic resonance imaging of cerebral associative white matter bundles employing fast-scan techniques. *Acta Anat (Basel)*. 158:215-221.
- Conturo TE, Lori NE, Cull TS, Akbudak E, Snyder AZ, Shimony JS, McKinstry RC, Burton H, Raichle ME. 1999. Tracking neuronal fiber pathways in the living human brain. *Proc Natl Acad Sci U S A*. 96:10422-10427.
- D'Arceuil H, de Crespigny A. 2007. The effect of brain tissue decomposition on diffusion tensor imaging and tractography. *Neuroimage*. 36:64-68.
- D'Arceuil H, Liu C, Levitt P, Thompson B, Kosofsky B, de Crespigny A. 2008. Three dimensional high-resolution diffusion tensor imaging and tractography of the developing rabbit brain. *Dev Neurosci*. 30:262-275.
- Dawe RJ, Bennet DA, Schneider JA, Vasireddi SK, Arfanakis K. 2009. Postmortem MRI of human brain hemispheres: t2 relaxation times during formaldehyde fixation. *Magn Reson Med*. 61:810-818.
- Engel AK, Muller CM. 1989. Postnatal development of vimentin-immunoreactive radial glial cells in the primary visual cortex of the cat. *J Neurocytol*. 18:437-450.
- Flechsig P. 1920. *Anatomie des menschlichen Gehirns und Rückenmarks auf myelogenetischer Grundlage*. Leipzig (Germany): G. Thieme.
- Friauf E, McConnell SK, Shatz CJ. 1990. Functional synaptic circuits in the subplate during fetal and early postnatal development of cat visual cortex. *J Neurosci*. 10:2601-2613.
- Ghosh A, Shatz CJ. 1992. Pathfinding and target selection by developing geniculocortical axons. *J Neurosci*. 12:39-55.
- Ghosh A, Shatz CJ. 1993. A role for subplate neurons in the patterning of connections from thalamus to neocortex. *Development*. 117:1031-1047.
- Hardy RJ, Friedrich VL Jr. 1996. Oligodendrocyte progenitors are generated throughout the embryonic mouse brain, but differentiate in restricted foci. *Development*. 122:2059-2069.
- Hermann K, Antonini A, Shatz CJ. 1994. Ultrastructural evidence for synaptic interactions between thalamocortical axons and subplate neurons. *Eur J Neurosci*. 6:1729-1742.
- Hermoye L, Saint-Martin C, Cosnard G, Lee SK, Kim J, Nassogne MC, Menten R, Clapuyt P, Donohue PK, Hua K, et al. 2006. Pediatric diffusion tensor imaging: normal database and observation of the white matter maturation in early childhood. *Neuroimage*. 29:493-504.
- Huang H, Xue R, Zhang J, Ren T, Richards LJ, Yarowsky P, Miller MI, Mori S. 2009. Anatomical characterization of human fetal brain development with diffusion tensor magnetic resonance imaging. *J Neurosci*. 29:4263-4273.
- Huang H, Yamamoto A, Hossain MA, Younes L, Mori S. 2008. Quantitative cortical mapping of fractional anisotropy in developing rat brains. *J Neurosci*. 28:1427-1433.
- Huang H, Zhang J, Wakana S, Zhang W, Ren T, Richards L, Yarowsky P, Donohue P, Graham E, van Zijl PCM, et al. 2006. White and gray matter development in human fetal, newborn and pediatric brains. *Neuroimage*. 33:27-38.
- Huppi PS, Maier SE, Peled S, Zientara GP, Barnes PD, Jolesz FA, Volpe JJ. 1998. Microstructural development of human newborn cerebral white matter assessed in vivo by diffusion tensor magnetic resonance imaging. *Pediatr Res*. 44:584-590.
- Innocenti GM, Frost DO. 1979. Effects of visual experience on the maturation of the efferent system to the corpus callosum. *Nature*. 280:231-234.
- Innocenti GM, Price DJ. 2005. Exuberance in the development of cortical networks. *Nat Rev Neurosci*. 6:955-965.
- Issa NP, Trachtenberg JT, Chapman B, Zahs KR, Stryker MP. 1999. The critical period for ocular dominance plasticity in the Ferret's visual cortex. *J Neurosci*. 19:6965-6978.
- Johnson JK, Casagrande VA. 1993. Prenatal development of axon outgrowth and connectivity in the ferret visual system. *Vis Neurosci*. 10:117-130.
- Jones DK, Simmons A, Williams SC, Horsfield MA. 1999. Non-invasive assessment of axonal fiber connectivity in the human brain via diffusion tensor MRI. *Magn Reson Med*. 42:37-41.
- Kier EL, Staib LH, Davis LM, Bronen RA. 2004. Anatomic dissection tractography: a new method for precise MR localization of white matter tracts. *Am J Neuroradiol*. 25:670-676.
- Kostovic I, Jovanov-Milosevic N. 2006. The development of cerebral connections during the first 20-45 weeks' gestation. *Semin Fetal Neonat Med*. 11:415-422.
- Kostovic I, Judas M, Rados M, Hrabac P. 2002. Laminar organization of the human fetal cerebrum revealed by histochemical markers and magnetic resonance imaging. *Cereb Cortex*. 12:536-544.
- Kostovic I, Rakic P. 1990. Developmental history of the transient subplate zone in the visual and somatosensory cortex of the macaque monkey and human brain. *J Comp Neurol*. 297:441-470.
- Kostovic I, Vasung L. 2009. Insights from in vitro fetal magnetic resonance imaging of cerebral development. *Semin Perinatol*. 33:220-233.
- Kretschmann HJ, Kammradt G, Krauthausen I, Sauer B, Wingert F. 1986. Brain growth in man. *Bibl Anat*. 28:1-26.
- Kroenke CD, Bretthorst GL, Inder TE, Neil JJ. 2005. Diffusion MR imaging characteristics of the developing primate brain. *Neuroimage*. 25:1205-1213.
- Kroenke CD, Van Essen DC, Inder TE, Rees S, Bretthorst GL, Neil JJ. 2007. Microstructural changes of the baboon cerebral cortex during gestational development reflected in magnetic resonance imaging diffusion anisotropy. *J Neurosci*. 27:12506-12515.
- Kuo L-W, Chen J-H, Wedeen VJ, Tseng WY. 2008. Optimization of diffusion spectrum imaging and q-ball imaging on clinical MRI system. *Neuroimage*. 41:7-18.
- Lin CP, Wedeen VJ, Chen JH, Yao C, Tseng WY. 2003. Validation of diffusion spectrum magnetic resonance imaging with manganese-enhanced rat optic tracts and ex vivo phantoms. *Neuroimage*. 19:482-495.
- Luskin MB, Shatz CJ. 1985. Neurogenesis of the cat's primary visual cortex. *J Comp Neurol*. 242:611-631.
- Maas LC, Mukherjee P, Carballido-Gamio J, Veeraraghavan S, Miller SP, Partridge SC, Henry RG, Barkovich AJ, Vigneron DB. 2004. Early laminar organization of the human cerebrum demonstrated with diffusion tensor imaging in extremely premature infants. *Neuroimage*. 22:1134-1140.
- Makris N, Worth AJ, Sorensen AG, Papadimitriou GM, Wu O, Reese TG, Wedeen VJ, Davis TL, Stakes JW, Caviness VS, et al. 1997. Morphometry of in vivo human white matter association pathways with diffusion-weighted magnetic resonance imaging. *Ann Neurol*. 42:951-962.
- Marin-Padilla M. 1992. Ontogenesis of the pyramidal cell of the mammalian neocortex and developmental cytoarchitectonics: a unifying theory. *J Comp Neurol*. 321:223-240.
- McKinstry RC, Mathur A, Miller JH, Ozcan A, Snyder AZ, Schefft GL, Almli CR, Shiran SI, Conturo TE, Neil JJ. 2002. Radial organization of developing preterm human cerebral cortex revealed by non-invasive water diffusion anisotropy MRI. *Cereb Cortex*. 12:1237-1243.
- McLennan JE, Gilles FH, Neff RK. 1983. A model of growth of the human fetal brain. In: Gilles FH, Leviton A, Dooling EC, editors. *The developing human brain: growth and Epidemiologic neuropathology*. Boston (MA): Wright.
- Miller SP, Vigneron DB, Henry RG, Bohland MA, Ceppi-Cozzio C, Hoffman C, Newton N, Partridge JC, Ferriero DM, Barkovich AJ. 2002. Serial quantitative diffusion tensor MRI of the premature brain: development in newborns with and without injury. *J Magn Reson Imaging*. 16:621-632.
- Mori S. 2007. *Introduction to diffusion tensor imaging*. 1st ed. Amsterdam, the Netherlands: Elsevier.
- Mori S, Crain BJ, Chacko VP, van Zijl PCM. 1999. Three-dimensional tracking of axonal projections in the brain by magnetic resonance imaging. *Ann Neurol*. 45:265-269.

- Mori S, Itoh R, Zhang J, Kaufmann WE, van Zijl PC, Solaiyappan M, Yarowsky P. 2001. Diffusion tensor imaging of the developing mouse brain. *Magn Reson Med.* 46:18-23.
- Neil JJ, Shiran SI, McKinstry RC, Schefft GL, Snyder AZ, Almlí CF, Akbudak E, Aronovitz JA, Miller JP, Lee BC, et al. 1998. Normal brain in human newborns: apparent diffusion coefficient and diffusion anisotropy measured by using diffusion tensor MR imaging. *Radiology.* 15:57-66.
- Neil JJ, Miller J, Mukherjee P, Huppi PS. 2002. Diffusion tensor imaging of normal and injured developing human brain—a technical review. *NMR Biomed.* 15:543-552.
- O'Leary DDM, Schlaggar BL, Tuttle R. 1994. Specification of neocortical areas and thalamocortical connections. *Annu Rev Neurosci.* 17:419-439.
- Paus T, Collins DL, Evans AC, Leonard G, Pike B, Zijdenbos A. 2001. Maturation of white matter in the human brain: a review of magnetic resonance studies. *Brain Res Bull.* 54:255-266.
- Pierpaoli C, Jezzard P, Basser PJ, Barnett A, Di Chiro G. 1996. Diffusion tensor MR imaging of the human brain. *Radiology.* 201:637-648.
- Prayer D, Barkovich AJ, Kirschner DA, Prayer LM, Roberts TP, Kucharczyk J, Moseley ME. 2001. Visualization of nonstructural changes in early white matter development on diffusion-weighted MR images: evidence supporting premyelination anisotropy. *Am J Neuroradiol.* 22:1572-1576.
- Remahl S, Hildebrand C. 1982. Changing relation between onset of myelination and axon diameter range in developing feline white matter. *J Neurol Sci.* 54:33-45.
- Remahl S, Hildebrand C. 1990. Relations between axons and oligodendroglial cells during initial myelination. II. The individual axon. *J Neurocytol.* 19:883-898.
- Rivkin MJ, Flax J, Mozell R, Osathanondh R, Volpe JJ, Villa-Komaroff L. 1995. Oligodendroglial development in human fetal cerebrum. *Ann Neurol.* 38:92-101.
- Rutherford MA, Cowan FM, Manzur AY, Dubowitz LM, Pennock JM, Hajnal JV, Young IR, Bydder GM. 1991. MR imaging of anisotropically restricted diffusion in the brain of neonates and infants. *J Comput Assist Tomogr.* 15:188-198.
- Sakuma H, Nomura Y, Takeda K, Tagami T, Nakagawa T, Tamagawa Y, Ishii Y, Tsukamoto T. 1991. Adult and neonatal human brain: diffusional anisotropy and myelination with diffusion weighted MR imaging. *Radiology.* 180:229-233.
- Schmithorst VJ, Wilke M, Dardzinski BJ, Holland SK. 2002. Correlation of white matter diffusivity and anisotropy with age during childhood and adolescence: a cross-sectional diffusion-tensor MR imaging study. *Radiology.* 222:212-218.
- Sidman RL, Rakic P. 1973. Neuronal migration, with special reference to developing human brain: a review. *Brain Res.* 62:1-35.
- Takahashi E, Dai G, Wang R, Ohki K, Rosen GD, Galaburda AM, Grant PE, Wedeen VJ. 2010. Development of cerebral fiber pathways in cats revealed by diffusion spectrum imaging. *Neuroimage.* 49:1231-1240.
- Ulfing N, Neudorfer F, Bohl J. 2000. Transient structures of the human fetal brain: subplate, thalamic reticular complex, ganglionic eminence. *Histol Histopathol.* 15:771-790.
- Van der Knaap MS, Valk J. 1990. MR imaging of the various stages of normal myelination during the first year of life. *Neuroradiol.* 31:459-470.
- Wedeen VJ, Hagmann P, Tseng WY, Reese TG, Weisskoff RM. 2005. Mapping complex tissue architecture with diffusion spectrum magnetic resonance imaging. *Magn Reson Med.* 54:1377-1386.
- Yakovlev PI, Lecours AR. 1967. The myelogenetic cycles of regional maturation in the brain. In: Minowski A, editor. *Regional development of the brain in early life.* Oxford: Blackwell. p. 3-69.
- Zhang J, Richards LJ, Yarowsky P, Huang H, van Zijl PCM, Mori S. 2003. Three dimensional anatomical characterization of the developing mouse brain by diffusion tensor microimaging. *Neuroimage.* 20:1639-1648.
- Zhang J, Chen Y, Hardwick JM, Miller MI, Plachez C, Richards LJ, Yarowsky P, van Zijl PCM, Mori S. 2005. Magnetic resonance diffusion tensor microimaging reveals a role for Bcl-x in brain development and homeostasis. *J Neurosci.* 25:1881-1888.